Prediction of ultimate strength of concrete walls restrained on three sides

Prediction of Ultimate Strength of Concrete Walls Restrained on Three Sides

Nhat-Minh Ho[1] and Jeung-Hwan Doh [1*]

[1] School of Engineering and Built Environment, Griffith University Gold Coast Campus, Queensland 4222, Australia

[*] Correspondence; Email: j.doh@griffith.edu.au

ABSTRACT

This paper presents experimental and numerical investigations on the behaviour of axially-loaded concrete walls restrained on three sides (TW3S walls). Particular emphasis was given to the influences of varying the slenderness ratio, aspect ratio, concrete strength, and eccentricity on the ultimate axial strength of TW3S walls. Because of the overly conservative nature of the code design equations and the scarcity of other available models for estimating the ultimate axial strength of TW3S walls, a more encompassing design equation has been developed. Comparisons with the test data of the current and previous studies confirmed that the proposed equation is satisfactory and reliable.

KEYWORDS: concrete wall, eccentric axial loading, slenderness ratio, aspect ratio, concrete strength

1. INTRODUCTION

Axially-loaded reinforced concrete (RC) walls can be supported at the bottom by a floor system and at the top by a roof structure or another floor (Figure 1a). Such walls behave in one-way action (OW), which deflects in a uniaxial curvature parallel to the load direction. In multistorey buildings, walls are usually combined to form a structure, such as an isolated box, a bundled box, a coupled core, or a geometric, U-, T-, or L-shape,[1] to make efficient use of building areas. With these configurations, walls may be laterally supported on one or both sides by interconnecting walls (Figures 1b, c). As a result, these lateral restraints transform the OW behaviour to two-way action (TW) behaviour, depicted by biaxial curvatures in both parallel and perpendicular directions to the load direction.

RC walls with eccentric axial loads can be designed using simplified design methods provided in codes, such as the Eurocode 2 (EC2-04),[2] the Australian Concrete Standard (AS3600-09),[3] and the American Concrete Institute Code (ACI318-14).[4] However, Popescu et al[5] highlighted that these code methods are considered conservative and can only be used if certain restrictions are met. Although numerous studies have been undertaken on OW walls and TW walls supported on four sides (TW4S walls), in an attempt to better understand the structural behaviour of such walls and to further improve their design models, the performance of TW walls supported on three sides (TW3S walls) has not been investigated to the same depth and there is little research published in this area. Apart from a number of tests carried out by Doh et al[6], and more recently by Ho and Doh[7], there has been a lack of fully comprehensive research on the axial load capacity of TW3S walls, and of design models for high slenderness TW3S walls with various aspect ratios. Consequently, there is a need for further studies on TW3S walls, which is the focus of this paper.

In the current study, a new experiment was designed, adding tests incorporating six one-third to one-half scale walls under eccentric axial loading. The main aim of this new experiment

was to study in greater detail the influence on the axial load capacity of TW3S walls of varying the slenderness ratio (H_w/t_w) and aspect ratio (H_w/L_w), which was not addressed in previous experimental studies. As it was not practical to conduct further experiments because of resource constraints, a finite element model (FE-Model) using the ABAQUS software was subsequently employed to thoroughly investigate the behaviour of TW3S walls. Extensive parametric studies were undertaken to examine the effects of key parameters on the ultimate axial strength of TW3S walls. Particular emphasis was given to the effects of varying the slenderness ratio (H_w/t_w), aspect ratio (H_w/L_w), concrete strength (f'_c), and eccentricity (e). The numerical results were then used to derive a new design equation which covers a broader spectrum of designs for TW3S walls.

2. SIMPLIFIED WALL DESIGN EQUATIONS IN CODES

The design equations stipulated in the three major codes, namely EC2-04[2], AS3600-09[3], and ACI318-14[4], to predict the design axial strength of a braced wall are shown in Table 1. The symbols used in these equations are defined in Notation.

While both EC2-04[2] and AS3600-09[3] include the effects of the restraints on the side edges through the effective height factor k (as specified in $H_{we} = kH_w$), ACI318-14[4] only takes into consideration restraints applied at the top and bottom of walls, and fails to recognise any contribution to load capacity from the side restraints. The factor k is given as follows:

a) For OW walls:

   k = 0.85 for EC2-04[2], k = 0.75 for AS3600-09[3], and k = 0.80 for ACI318-14[4], when walls are restrained against rotation at both ends; and

   k = 1.0 for all three major codes, when walls are not restrained against rotation at one or both ends.

b) For TW3S walls:

$k = \frac{1}{1+(H_w / 3L_w)^2}$ for both EC2-04[2] and AS3600-09[3]. However AS3600-09[3] further specifies that the value of k is not less than 0.3.

c) For TW4S walls:

$$k = \frac{1}{1+(H_w / L_w)^2} \text{ when } H_w \le L_w$$
$$k = \frac{L}{2H_w} \text{ when } H_w > L_w$$

for both EC2-04[2] and AS3600-09[3].

3. EXPERIMENTAL PROGRAMME

In an effort to undertake a comparison study with experimental results from previous research,[6,7] six one-third to one-half scale wall panels with various slenderness ratios (H_w/t_w) and aspect ratios (H_w/L_w) were cast and tested to failure.

All panels were cast horizontally in purpose-made timber moulds with minimum central reinforcement ($\rho_v = \rho_h = 0.31\%$). A single F41 mesh centrally placed within the panel cross-section allowed the elements to be treated as unreinforced elements, with no contribution to their capacity from the steel reinforcement.[7] The primary purpose of minimum wall reinforcement detailing was to control cracking due to shrinkage and temperature stresses. The design yield strength and the minimum tensile strength of the F41 mesh are 450 and 500 MPa, respectively. The concrete was supplied by a local concrete ready-mix company. General purpose cement, sand, and maximum 10 mm aggregates were used to produce the concrete with a specific slump of 80 mm. The average compressive strength of the concrete utilised for the panels was determined by standard-sized concrete cylinders cured under the same moist-curing condition beside the panels. The geometric and material properties of the test panels (and those conducted by Doh et al[6], and Ho and Doh[7]) are given in Table 2.

For consistency, the test set-up and procedure, as described in previously published papers,[6,7] were employed. The arrangement of the test set-up is shown in Figure 2. The panels were simply supported on three sides under as-built restraints. Details of the simply supported top-hinged and side-hinged edges are shown in Figures 3 and 4, respectively. The out-of-plane displacements of the wall panels during testing were measured by four linear variable differential transformers (LVDTs). They were attached to the compression face of the walls (Figure 5). A static loading regime was adopted for the testing. A load cell was positioned between the centre hydraulic jack and the upper loading beam. The walls were loaded in increments until failure. At each load increment, crack patterns and deflections were recorded.

4. EXPERIMENTAL RESULTS

4.1. Failure modes and crack patterns

No crack was observed until failure for all specimens. The walls exhibited brittle failure which was due to the initial eccentric loading being enhanced by the P-Delta effect induced during testing. Typical double curvature bending failure was evident as a result of the walls' being supported on three sides. The crack patterns on the tension and compression faces of the test specimens, after failure, are presented in Figure 6. Generally, there was a transition of cracking characteristics of the walls, which occurred with higher aspect ratio. Specifically, the crack patterns of the WS1a and W1b panels showed the development of diagonal cracking from the two restrained corners, together with horizontal cracking propagation from the unrestrained edge, which all converged (Figures 6a, c). This particular cracking mode indicates two-way behaviour close to the restrained end and one-way behaviour close to the free end. Conversely, the crack patterns of the WS1c, WS2a and WS2b panels were evidently dominated by two-way behaviour characterised by only the propagation of diagonal cracking from the two restrained corners (Figures 6e, g, i). This may be due to the lateral boundary condition becoming more

active once the aspect ratio of the wall increases. For all specimens, the diagonal cracks developed at roughly 35-50^o inclination from the top and bottom corners. Several smeared cracks appeared around the major cracks. There was concrete crushing on the compression face along the major cracks and concrete spalling near the top or bottom edges.

4.2. Axial load – deflection relationship

Figure 7 shows load versus lateral deflection responses for the selected test panels. The panels failed in a brittle mode in which they were unable to sustain any further loading after reaching the maximum load. All curves were generally linear for the initial load regions, followed by nonlinear trends with the deflections increasing rapidly as the failure was approached. This rapid increase commenced at around 40% to 60% of the ultimate loads.

4.3. Ultimate strength

ACI318-14[4] does not provide the methodology to account for the increase in axial load capacity of walls due to the presence of side restraints, thus Equation (3) was excluded from the comparison of test results. The comparison of the predicted failure loads from the two other applicable code equations, Equations (1) and (2), with the test results of the 12 wall panels is given in Table 3. As indicated in Table 3, the code equations failed to adequately predict the ultimate capacity of the high slenderness wall panels with various aspect ratios. For instance, when H_w/t_w = 35 and 40, these equations yielded very conservative or negative values (zero load-carrying capacity), which was clearly inaccurate as the actual test results produced significant load capacities for these panels. Regarding EC2-04[2], the ratios of predicted to actual strength ranged between 0.21 and 0.78, with an overall mean of 0.55, and a standard deviation of 0.21. Concerning AS3600-09[3], the ratios of predicted to actual strength varied from 0.07 to 1.01, with an overall mean of 0.71, and a standard deviation of 0.27. If the capacity reduction

factor, ϕ, (ϕ = 0.67 for EC2-04[2], and ϕ = 0.6 AS3600-09[3]) is used in the design, then Equations (1) and (2) provide safe but overly conservative design values.

To observe the effects of aspect ratio (H_w/L_w) and slenderness ratio (H_w/t_w) of TW3S walls closely, the axial strength ratios ($N_u/f'_cL_wt_w$) of test data, including the current test failure load points and the test results from previous research,[6,7] were plotted against these parameters (Figures 8 and 9). The failure lines, predicted by the EC2 and AS3600 equations, were also plotted in these figures. As indicated in Figure 8, the axial strength ratio was found to gradually increase with increasing aspect ratio. The increase in the axial strength ratio in panels with H_w/t_w = 25 was approximately 52.4%, when H_w/L_w was increased from 0.83 to 1.6. Further, the increase in the axial strength ratio in panels with H_w/t_w = 30 was approximately 49.2%, when H_w/L_w was increased from 1.0 to 2.0. Significantly, Saheb and Desayi[8] reported that the ultimate strength of the OW wall panels decreased linearly with increasing aspect ratio (an increase in H_w/L_w from 0.67 to 2.0). In general, these results indicate that the axial strength ratio of OW and TW3S walls shows a divergent trend when the aspect ratio increases, highlighting the perceived advantages gained from having a side restraint. This further implies that, although it is safe to design TW3S walls as OW walls, this may be too conservative and uneconomical because of the requirement for a significant amount of construction material and the cost of building construction in many scenarios. Accordingly, considerable savings may be attained if an accurate, less conservative design of RC walls can be produced. As seen in Figure 9, as the slenderness ratio increased, a decreasing trend in the axial strength ratio occurred. The reduction in the axial strength ratio was approximately 39.6% for an increase in H_w/t_w from 25 to 40, when H_w/L_w was kept constant and equal to 1.6. Figure 8a further highlights that the AS3600 failure line (Equation (2) line) safely predicts and appears to follow the general trend of the test results of walls with H_w/t_w = 25 along with a variation in H_w/L_w from 0.83 to 1.6.

However, the predicted failure lines of code equations showed a more dramatic rate of fall-off in axial strength, compared with the test data, for most of the remaining cases.

5. FINITE ELEMENT MODEL

5.1. Overview of the FE-Model

Experimental tests on only 12 specimens are insufficient to draw quantitative conclusions about the axial load capacity of TW3S walls. A numerical analysis of axially-loaded TW3S walls using the finite element ABAQUS program was thus conducted. The ABAQUS program was chosen for the finite element analysis because of its widely-known ability to perform nonlinear analyses for RC members.[7,9-11] The FE-Model, which was developed in the previous study by Ho and Doh[7] for predicting the behaviour of RC walls with various support conditions under eccentric axial loading, was utilised in this research. Concrete was modelled using the concrete damage plasticity (CDP) model. Eight-node brick elements with reduced integration and hourglass control (C3D8R elements) were used to model the concrete wall and the restraints. Discrete truss elements in linear order (T3D2 elements) were used to model the steel reinforcement. The reinforcement was embedded in the concrete region with a perfect bond. The rough friction formulation was implemented in order to prevent the wall from losing contact with the restraints, so that boundary conditions could be correctly applied. In accordance with the hard contact simulation used, both the RC wall and the restraints were assumed to be impenetrable rigid bodies. The modified Riks method, which is usually used to predict the unstable, geometrically nonlinear collapse of a structure and can include the nonlinear materials, was employed to analyse all the numerical models for the purpose of finding the ultimate strength of the walls. Automatic stability was used to avoid divergence solutions, and the Nlgeom was activated to account for the geometric nonlinearity. Full details of the numerical modelling techniques can be found in the published study.[7]

5.2. Comparative study

The effectiveness of the numerical simulations was demonstrated through a comparison with the experimental results obtained in this research and in the previous studies[6,7] with respect to crack patterns, load-deflection responses, and ultimate loads. In the numerical models, the crack patterns were visualised through the maximum principal plastic strains. Figure 10 shows typical examples of the crack patterns reasonably well predicted by the numerical simulations. The comparison of the load-deflection response between the experimental and numerical results is shown in the aforementioned Figure 7. The trends of the load-deflection responses in the experimental tests and numerical models were similar. However, the gradients of the load-deflection responses predicted by the FE-Model were slightly steeper than those of the experimental results. The ultimate loads predicted by the FE-Model are presented in Table 3. The FE ultimate load predictions ($N_{uw,FE\text{-}Model}$) were satisfactory but slightly overestimated. The results indicated that the ratios of the FE analysis to experimental failure loads ($N_{uw,FE\text{-}Model}/N_{uw,Test}$) varied from 0.95 to 1.24, with a mean of 1.09, and a standard deviation of 0.11. These discrepancies are expected due to the experimental errors associated with the materials, the test set-up and measurements, along with the idealistic nature of the FE-Model.

In general, the numerical simulations showed close correlation with the experimental observations. The modelling techniques adopted to simulate the wall panels are thus proven to be satisfactory, and can be employed to carry out further investigations.

5.3. Parametric study

A series of parametric studies was performed to study the influences of slenderness ratio (H_w/t_w), aspect ratio (H_w/L_w), concrete strength (f'_c), and eccentricity (e) on the axial load capacity of TW3S walls. The walls were 3000 mm in height and the length of the walls varied

from 1000 to 10 000 mm. The thickness of the walls varied from 60 to 150 mm. Four different eccentricities ($e = t_w/20$, $t_w/6$, $t_w/4$, and $t_w/3$), and four different concrete strengths (f'_c = 32, 50, 80, and 100 MPa) were investigated. Each concrete wall model had a single layer of steel reinforcement, assumed to contain 12 mm diameter reinforcement bars, with a yield stress of 450 MPa, centrally placed with $\rho_v = \rho_h = \rho = 0.31\%$. The following observations were made.

5.3.1. Effect of the slenderness ratio

Figures 11-13 plot the axial strength ratio ($N_u/f'_cL_wt_w$) against slenderness ratio (H_w/t_w), with various eccentricities and concrete strengths. The slenderness ratio varied from 20 to 50 with H_w/L_w equal to 0.5, 1.0 and 2.0 being investigated. These figures indicate that the axial strength ratio decreased nonlinearly with an increase in slenderness ratio due to the geometric nonlinear effect accelerating the failure of the panels. Further, when eccentricity was equal to $t_w/20$, decreases in axial strength ratio with increases in slenderness ratio were illustrated by the convex form of the curves in Figures 11a, 12a, and 13a. However, when eccentricity was greater than $t_w/20$, the curves converted to the concave form, as shown in Figures 11b-d, 12b-d, and 13b-d. At a fixed slenderness, the axial strength ratio was very sensitive to changes in eccentricity, and dramatically decreased with increases in eccentricity because of the collapse state of the wall panel being predominantly governed by buckling. For example, at $H_w/t_w = 20$ and f'_c = 32 MPa, when eccentricity increased from $t_w/20$ to $t_w/3$, the axial strength ratio decreased by 63.8%, 55.9%, and 49.6% for walls with H_w/L_w = 0.5, 1.0, and 2.0, respectively. Likewise, at $H_w/t_w = 50$ and f'_c = 100 MPa, the axial strength ratio reduced by 62.8%, 63.1%, and 63.0% for walls with H_w/L_w = 0.5, 1.0, and 2.0, respectively. Interestingly, the rates of decrease in the axial strength ratio for eccentricities of $t_w/20$ and $t_w/6$ were significant over the investigated range of slenderness ratios. However, in the case of the eccentricity of $t_w/3$, this rate of change was less intense in comparison with the other eccentricities.

5.3.2. Effect of the aspect ratio

To investigate the effect of aspect ratio, which varied from 0.3 to 3.0, all panels were subjected to a constant eccentricity of $t_w/6$. Figure 14 shows the axial strength ratio ($N_u/f'_cL_wt_w$) versus aspect ratio (H_w/L_w), with various concrete strengths of four different slenderness ratios (H_w/t_w = 20, 30, 40, and 50). As can be seen in Figure 14, the axial strength ratio increased nonlinearly and significantly with an increase in aspect ratio. For example, in the case of the f'_c = 32 MPa wall panels, when H_w/L_w increased from 0.3 to 3.0, the axial strength ratio increased by 51.7% for H_w/t_w = 20, whereas the axial strength ratio increased dramatically by 217.0% for H_w/t_w = 50. This may be due to the boundaries becoming more active when the aspect ratio of the wall increases, thereby utilising the strength of the material more effectively. Of note, the lateral boundary conditions are one of the parameters that influence the axial strength of a panel via the effective height factor. Once the aspect ratio of the wall increases, the effective height factor decreases, and therefore diminishes the slenderness effect.[12]

5.3.3. Effect of the concrete strength

The results from Figure 12 were converted into Table 4 to provide insights into the influence of concrete strength on the wall strength. Table 4 presents the ultimate strength increments due to concrete strengths with varying eccentricities for the walls with H_w/L_w = 1.0. It was found that the percentage increase in the wall strength did not correspond to the same percentage increase in the concrete strength. For example, when the concrete strength increased from 32 to 50 MPa (a 56.3% increase), from 50 to 80 MPa (a 60% increase), and from 80 to 100 MPa (a 25% increase), the wall strength increased by approximately 20% to 38%, 18% to 34%, and 7% to 15%, respectively. When considering the walls at H_w/t_w = 20 and $e = t_w/6$, an increase in the concrete strength from 32 to 100 MPa (a 212.5% increase) resulted in a much lower percentage increase in the wall strength, which was approximately 98.9%. Additionally, when doubling the concrete strength from 50 to 100 MPa (a 100% increase), only a 49.8% increase

in the wall strength was achieved. These observations are anticipated because high-strength concrete is structurally a distinct material and rules relevant to normal-strength concrete are not always conservative when applied to high-strength concrete.[13] Recall that the AS3600 equation showed a good prediction of failure load for the wall with the concrete strength of roughly 50 MPa at H_w/t_w = 25 and e = t_w/6 (see Section 4.3). The implication is that overestimation of the ultimate strength may occur when high-strength concrete is employed, even if the strength reduction (ϕ = 0.6) is used in design. The use of linear extrapolation for high-strength concrete in the current design codes is thus considered inappropriate, and may lead to highly unsafe designs.

In addition, a study of the walls with H_w/L_w = 0.5 and 2.0 resulted in similar observations to those of H_w/L_w = 1.0, illustrating the inapplicability of the linear relationship for concrete strength used in the code equations.

6. PROPOSED ULTIMATE LOAD PREDICTION EQUATION FOR TW3S WALLS

In view of the shortcomings of the code design equations and the scarcity of other available models to estimate the ultimate load capacity of TW3S walls, a new design equation, covering a broader spectrum of designs, was proposed in this study.

6.1. Development of the equation

Fragomeni and Doh[14] highlighted that the AS3600 equation was originally derived from a wall design equation only intended for OW walls, given in the British Concrete Standard (BS8110-97)[15]. The equation is expressed as $N_d = 0.3(t_w - 1.2e - 2e_a)f_{cu}$. The differences are attributed to the use of cube strength, f_{cu}, rather than cylinder strength, f'_c, with further variations in load and material factors used. Full derivation details are provided by Fragomeni[16]. The additional eccentricity, e_a, is given in the column design section in BS8110[15] as $e_a = \alpha(1/2000)(H_{we}/t_w)^2 t_w$, where α is a reduction factor applied to the deflection to allow for

the influence of axial load. In the case of walls, α is taken as 0.8;[15] therefore, for design purposes, the equation becomes $e_a = (H_{we})^2/2500t_w$. In order to account for the design of concrete walls with various support conditions, the effective height factors, k, which originated from the German Concrete Code (DIN 1045-88)[17], were later incorporated into the Australian Standard, which is the current AS3600-09[3]. According to Fragomeni[16], the German Code[17] utilised the plate buckling theory to obtain these effective height factors.

Scrutinising all the above-mentioned information, the conservative nature of the AS3600 equation could be attributed to the selected value of α. Hence, it is recommended that the parameter α should be modified, considering the effect of geometric characteristics, to compensate for the increased load capacity of TW3S walls. Based on this finding, and previous research outcomes, together with the experimental and numerical results presented in previous sections, the following assumptions were involved in the development of the proposed wall design equation:

a) The wall panel contains at least the minimum amount of steel reinforcement in both vertical and horizontal directions, as specified in AS3600-09[3].
b) An exponential value of 0.45 of concrete strength, f'_c, is suggested to give a safe prediction of wall strength, and to reflect the nonlinear increase in wall strength as concrete strength increases.
c) The parameter α, which has been calibrated from the FE-Model results using regression analysis, is defined as $\alpha = 0.8[50/(H_w/t_w)^{1.26}]$, leading to $e_a = [1/(H_w/t_w)^{1.26}] \times (H_{we}^2/50t_w)$, where $H_{we} = kH_w$, and $k = 1/[1 + (H_w/3L_w)^2]$.
d) The relationship of the axial strength ratio ($N_u/f'_cL_wt_w$) and the eccentricity (e) for walls when the slenderness ratio (H_w/t_w) approaches zero, is presented in Table 5. These values could be referred to as the strength limits in the design for walls with various eccentricities. Details of the full derivation are provided by Doh[18].

By incorporating the above assumptions and relevant parameters prescribed in the AS3600-09 equation, the following ultimate axial strength equation is proposed:

$$N_u = 4.5 f_c^{'0.45} L_w (t_w - 1.2e - 2e_a) \quad (4)$$

6.2. The performance of proposed equation

The aforementioned Table 3 also compared the failure load predicted by the proposed equation with the experimental results. The ratio of predicted strength to actual strength varied from 0.77 to 1.01, with an overall mean of 0.92 and a standard deviation of 0.07, indicating safe predictions when using Equation (4).

The aforementioned Figures 8 and 9 also provide further in-depth performance of the proposed Equation (4). These figures show the axial strength ratios that were obtained with the concrete strengths of 40, 50, and 60 MPa using Equation (4) with respect to H_w/L_w and H_w/t_w. An eccentricity equal to $t_w/6$ was used in all cases, and steel reinforcement ratios were assumed to be $\rho_v = \rho_h = \rho = 0.31\%$. All these values were chosen so that the test results could be closely compared. As seen in these figures, the proposed Equation (4) lines agree well with the general trend of the test results. The effect of the concrete strength on the axial strength ratio is also reflected, and contrasts with the linear relationship suggested by the code equations.

Overall, the proposed equations were deemed satisfactory considering that the test data from the current research programme and past research studies involved wall panels with varying slenderness ratio, aspect ratio, and concrete strength. With the use of an appropriate strength reduction factor, ϕ, in the design (e.g., $\phi = 0.6$ in AS3600-09[3]), Equation (4) provided safe and conservative predictions for all panels tested.

7. CONCLUSIONS

To date, the behaviour of axially-loaded TW3S walls has remained largely unexplored. To enhance the understanding of the structural behaviour of such walls, experimental and numerical investigations were carried out in this study. In addition, this study proposed a new design equation to predict the ultimate axial strength of TW3S walls. Comparisons with the available test results confirmed that the proposed equation is satisfactory and reliable. Since available models for estimating the axial load capacity of TW3S walls are rare, this proposed model can serve as a useful design aid for engineering applications.

NOTATIONS

e	eccentricity to account for eccentricity of the load application
e_a	eccentricity to account for slenderness and 'out of straightness'
f'_c	cylinder compressive strength of concrete
f_{cu}	cube compressive strength of concrete
H_w	floor-to-floor height of the wall
H_{we}	effective height of the wall ($H_{we} = kH_w$)
k	effective height factor
L_w	horizontal length of the wall
N_d	design axial strength
N_u	ultimate axial strength
t_w	thickness of the wall
α	reduction factor applied to the deflection to allow for the influence of axial load
Φ	specific load-bearing capacity for plain concrete walls
γ_c	partial safety factor
ϕ	capacity reduction factor
ρ	reinforcement ratio in the wall
ρ_h, ρ_v	horizontal and vertical reinforcement ratios in the wall, respectively

REFERENCES

1. Menegon, S.J., Wilson, J.L., Lam, N.T.K. and Gad, E.F.: RC walls in Australia: reconnaissance survey of industry and literature review of experimental testing. Australian Journal of Structural Engineering, 2017, vol. 18, pp. 24-40.
2. EN1992-1-1: Eurocode 2: design of concrete structures – Part 1–1: General rules and rules for buildings, Brussels: Comité Européen De Normalisation, 2004.
3. AS3600: Concrete structures, Sydney, Australia: Standards Australia, 2009.
4. ACI318: Building code requirements for structural concrete and commentary (ACI 318–14), Farmington Hills: American Concrete Institute, 2014.
5. Popescu, C., Sas, G., Blanksvärd, T. and Täljsten, B.: Concrete walls weakened by openings as compression members: a review. Engineering Structures, 2015, vol. 89, pp. 172–190.
6. Doh, J.H., Lee, D.-J., Guan, H. and Loo, Y.C.: Concrete wall with various support conditions. Proceedings of the 4th International Conference on Advances in Structural Engineering and Mechanics (ASEM'08), Korea, 2008.
7. Ho, N.M. and Doh, J.H.: Experimental and numerical investigations of axially loaded RC walls restrained on three sides. The Structural Design of Tall and Special Buildings, 2018. DOI: 10.1002/tal.1459.
8. Saheb, S.M. and Desayi, P.: Ultimate strength of RC wall panels in one-way in-plane action. Journal of Structural Engineering, 1989, vol. 115, pp. 2617–2630.
9. Lima, M.M., Doh, J.H. and Hadi, M.N.S.: The effects of CFRP orientation on the strengthening of reinforced concrete structures. The Structural Design of Tall and Special Buildings, 2016. DOI: 10.1002/tal.1282.
10. Lu, X.L., Wang, L., Wang, D. and Jiang, H.J.: An innovative joint connecting beam for precast concrete shear wall structures. Structural Concrete, 2016. DOI: 10.1002/suco.201500193.
11. Delnavaz, A. and Hamidnia, M.: Analytical investigation on shape configuration of CFRP strips on lateral loading capacity of strengthened RC shear wall. Structural Concrete, 2016. DOI: 10.1002/suco.201500196.
12. Popescu, C., Sas, G., Sabău, C. and Blanksvärd, T.: Effect of cut-out openings on the axial strength of concrete walls. Journal of Structural Engineering, 2016. DOI: 10.1061/(ASCE)ST.1943-541X.0001558.
13. Mendis P.: Design of high-strength concrete members: state-of-the-art. Progress in Structural Engineering and Materials, 2003, vol.5, pp. 1-15.

14. Fragomeni, S. and Doh, J.H.: Evaluation of the simplified concrete wall design equation in AS3600-2009. Australian Journal of Structural Engineering, 2010, vol. 10, pp. 253-262.
15. BS8110: Structural use of concrete, Part 1 – Code of practice for Design and Construction, London: British Standards Institution, 1997.
16. Fragomeni, S.: Design of normal and high strength reinforced concrete walls. PhD Thesis, University of Melbourne, Melbourne, Australia, 1995.
17. DIN 1045: Reinforced concrete structures: design and construction, Berlin: DIN (Deutsches Institut für Normung), 1988.
18. Doh, J.H.: Experimental and theoritical studies on normal and high strength concrete wall panels. PhD Thesis, Griffith University, Gold Coast, Australia, 2002.

LIST OF FIGURES

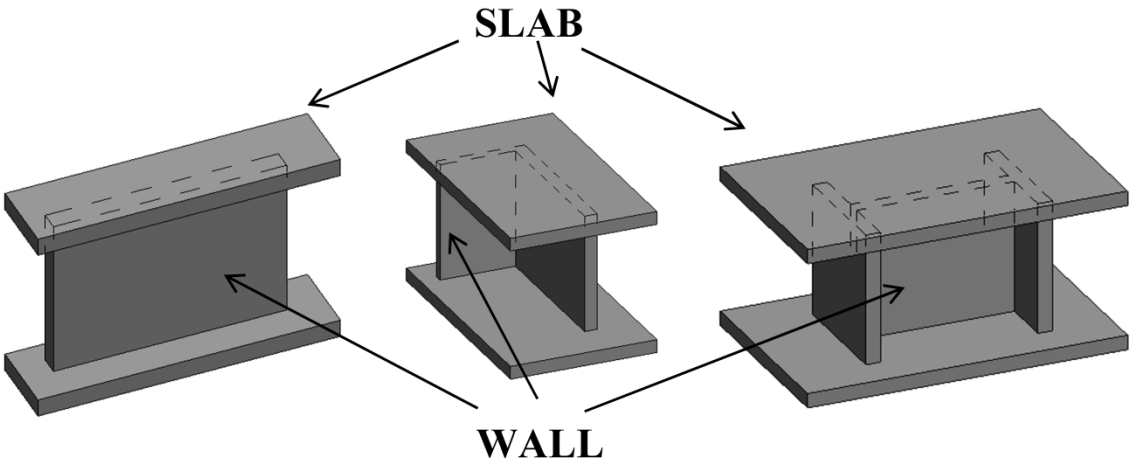

(a) One-way action (OW) (b) Two-way action supported on three sides (TW3S) (c) Two-way action supported on four sides (TW4S)

FIGURE 1 Walls with various support conditions

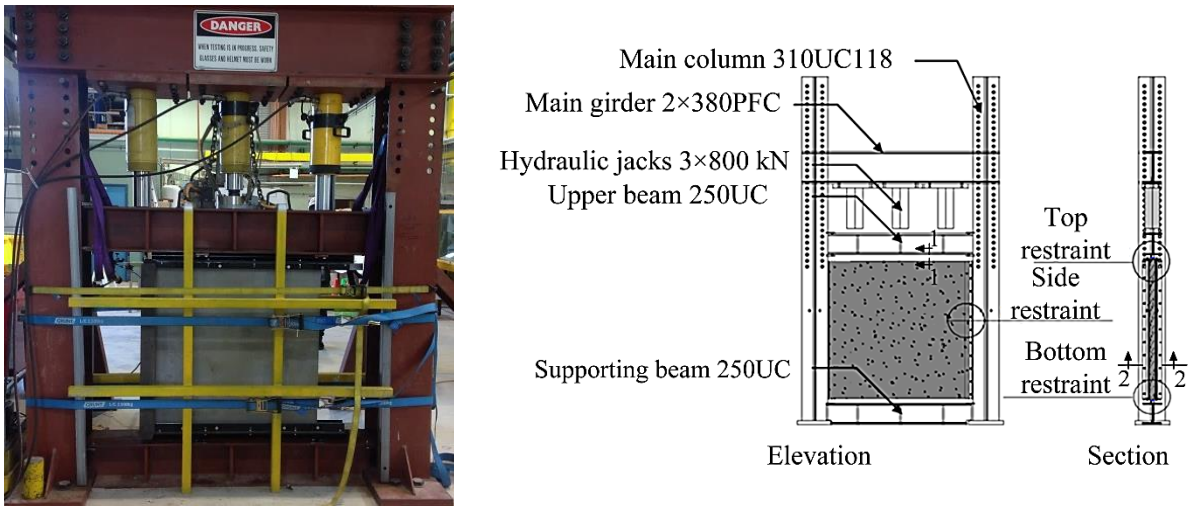

(a) Test frame arrangement (b) Schematic view of test set-up

FIGURE 2 Test rig set-up

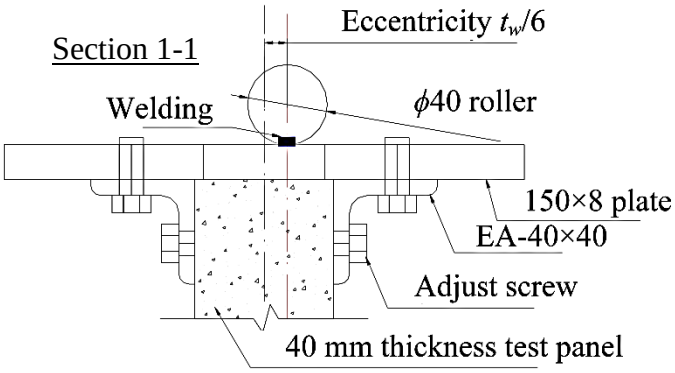

(a) Top restraint (b) Schematic view of top restraint

FIGURE 3 Top-hinged edge restraint

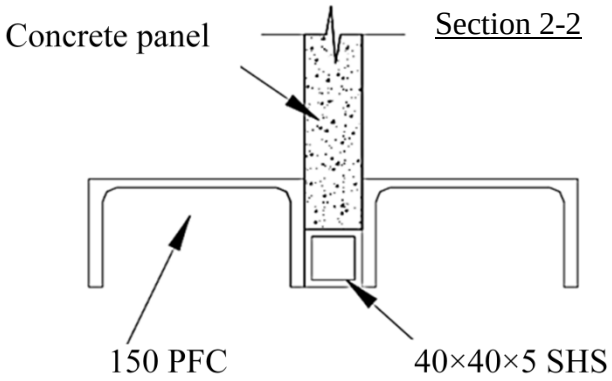

(a) Side restraint (b) Schematic view of side restraint

FIGURE 4 Side-hinged edge restraint

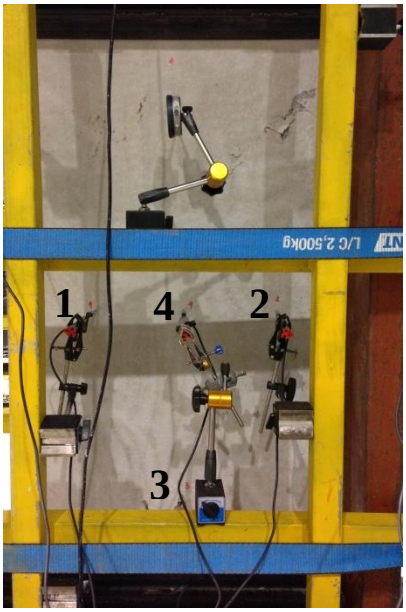

FIGURE 5 Arrangement of LVDTs on compression face

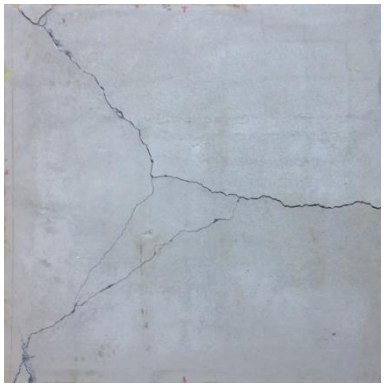

(a) Wall WS1a tension face

(c) Wall WS1b tension face

(e) Wall WS1c tension face

(b) Wall WS1a compression face

(d) Wall WS1b compression face

(f) Wall WS1c compression face

1

(g) Wall WS2a tension face

(i) Wall WS2b tension face

(k) Wall WS3a tension face

(h) Wall WS2a compression face

(j) Wall WS2b compression face

(l) Wall WS3a compression face

2 **FIGURE 6** Crack patterns of test specimens

3

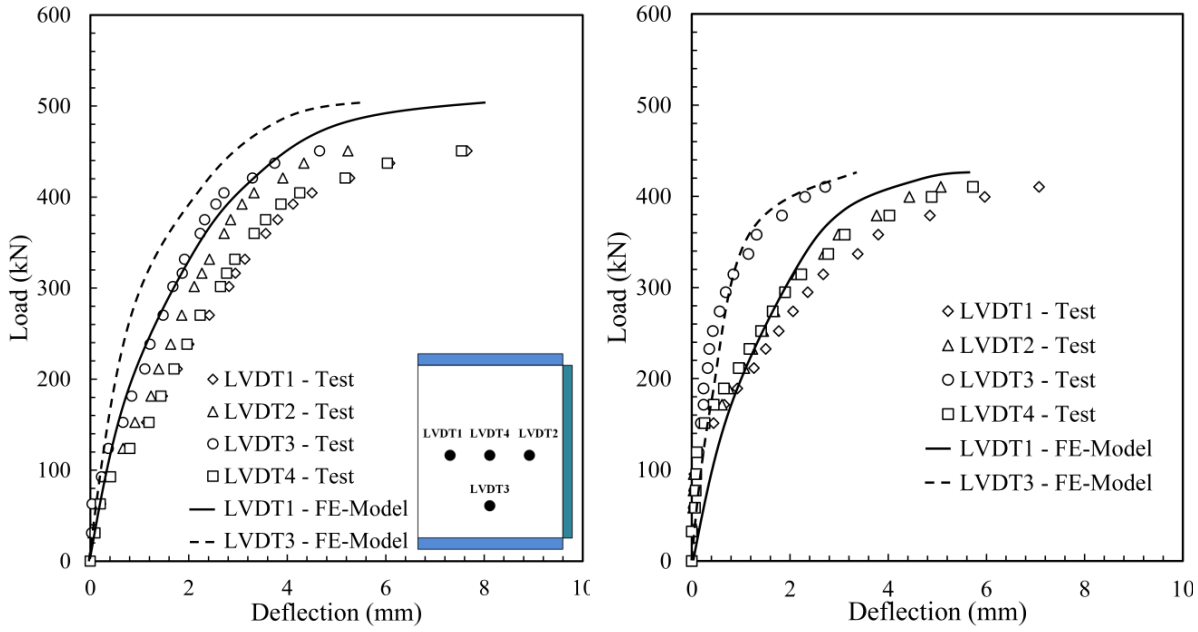

(a) WS1b (b) WS2a

FIGURE 7 Axial load – displacement relationship

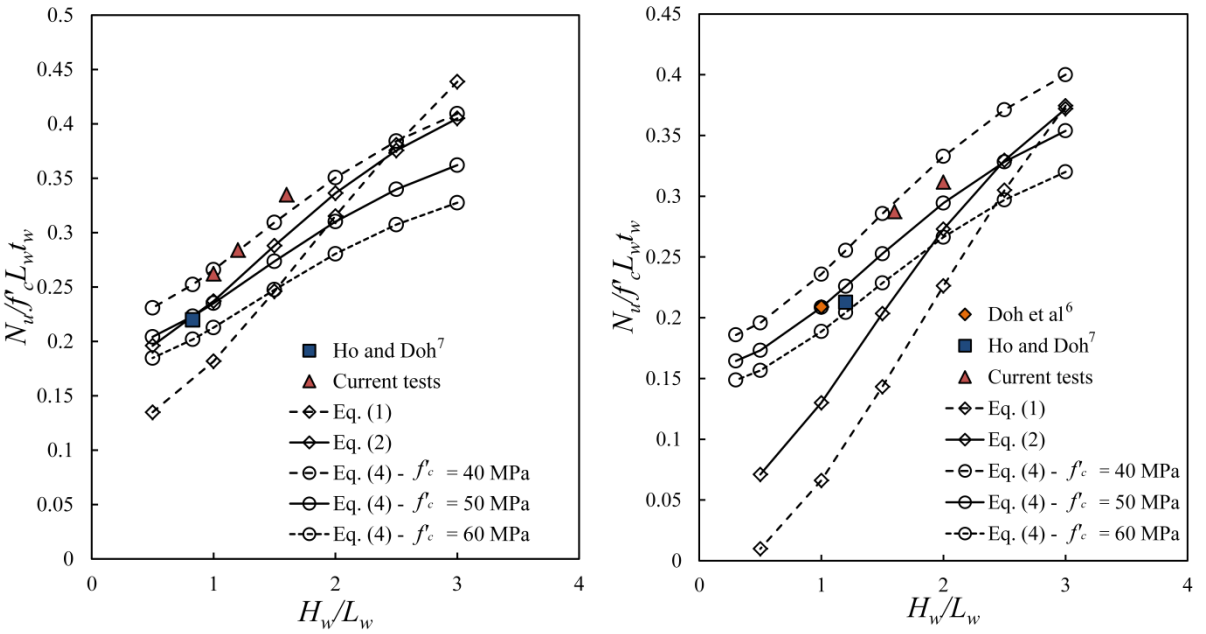

(a) H_w/t_w = 25 (b) H_w/t_w = 30

FIGURE 8 Prediction trends of wall equations for various aspect ratios

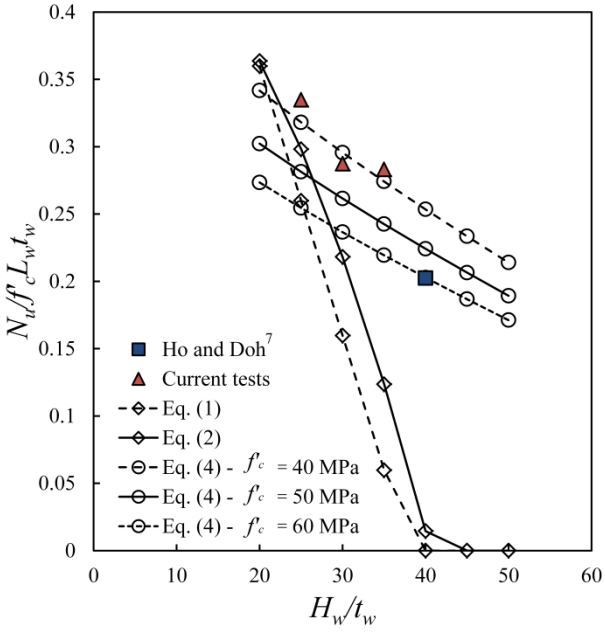

FIGURE 9 Prediction trends of wall equations for various slenderness ratios (H_w/L_w = 1.6)

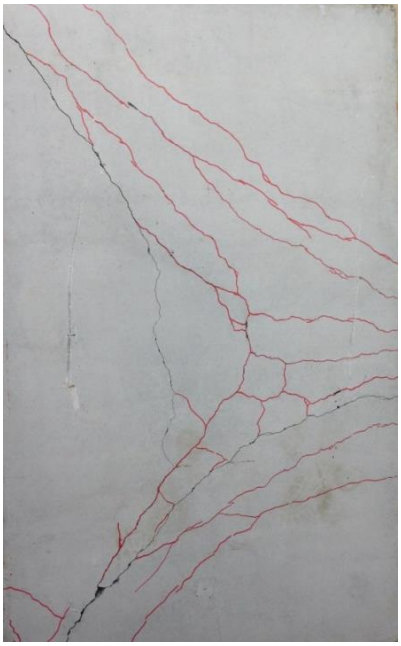

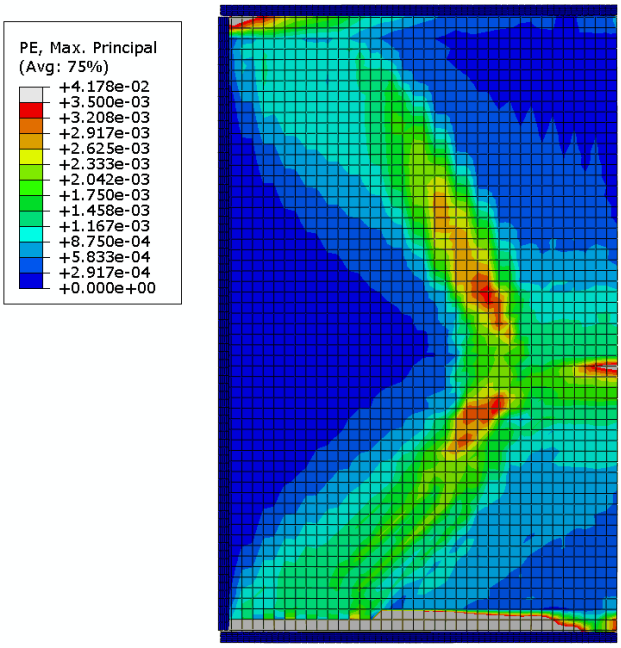

Experiment Maximum principal plastic strains

(a) WS4[7]

1

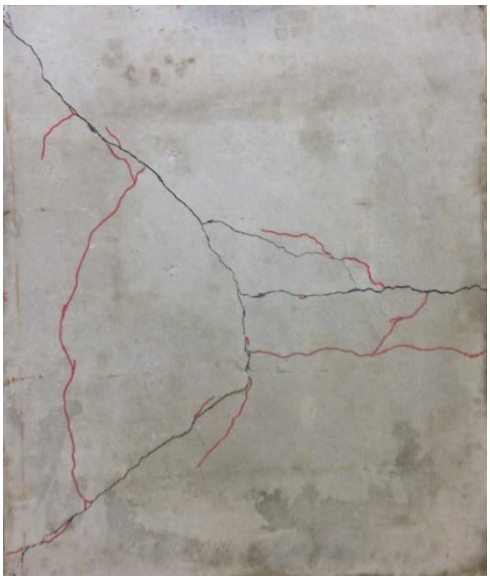

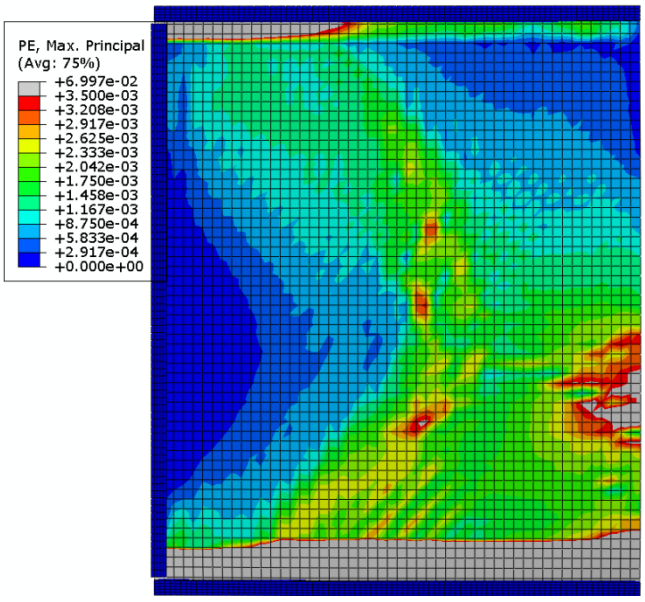

Experiment Maximum principal plastic strains

(b) WS1b

2

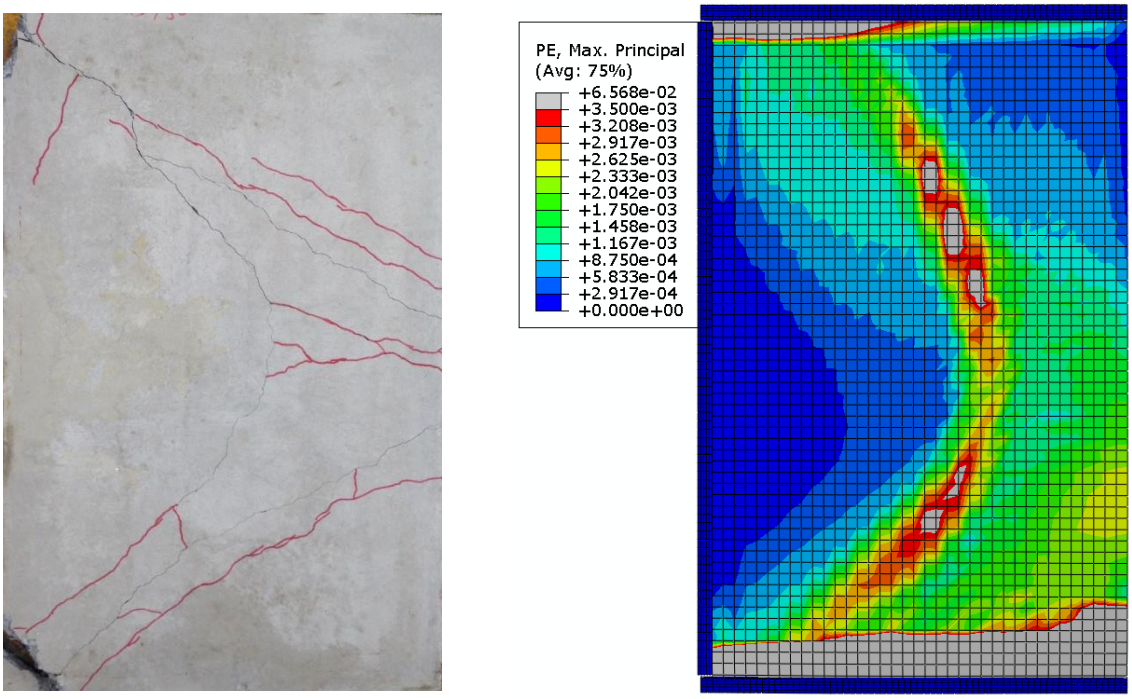

Experiment Maximum principal plastic strains

(c) WS2a

FIGURE 10 Crack patterns at ultimate load visualised through the maximum principal plastic strains

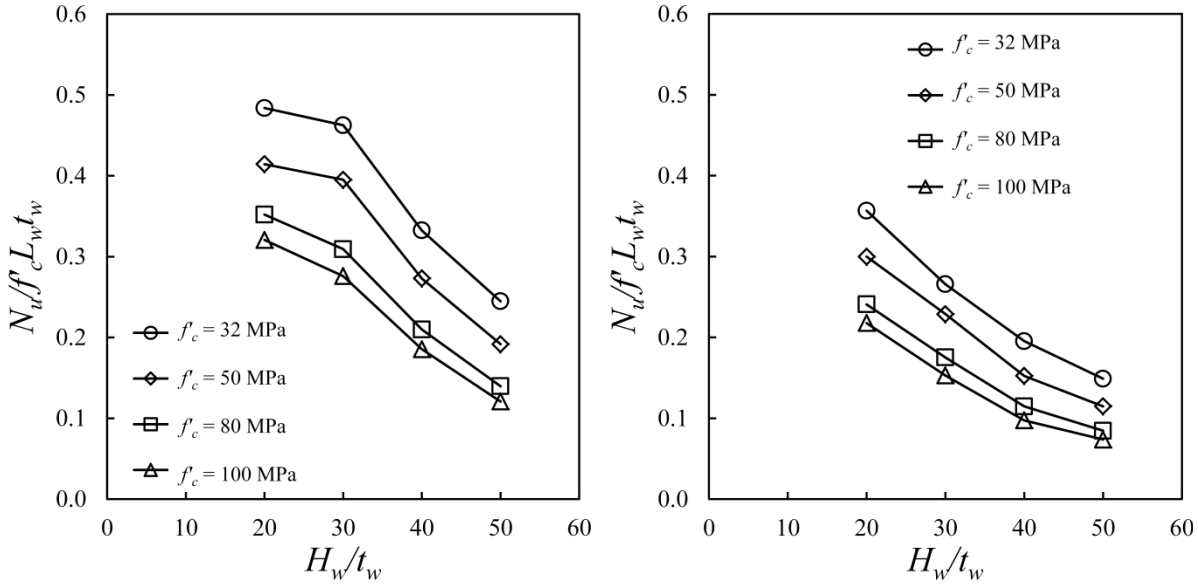

(a) $e = t_w/20$ (b) $e = t_w/6$

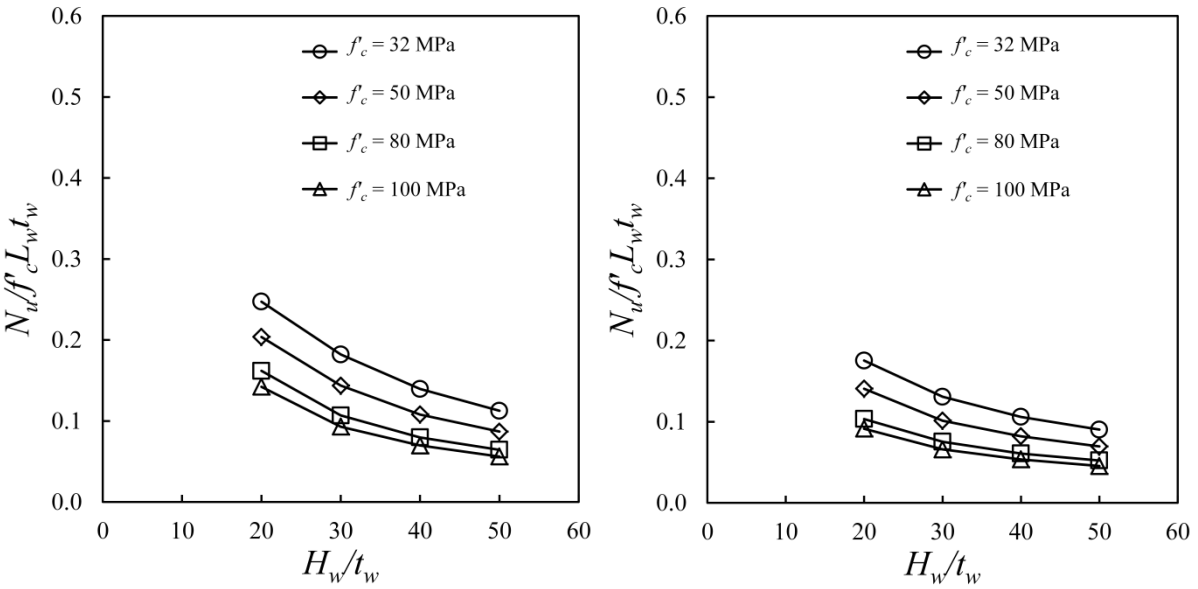

(c) $e = t_w/4$ (d) $e = t_w/3$

FIGURE 11 Axial strength ratio versus slenderness ratio (H_w/L_w = 0.5, ρ = 0.31%)

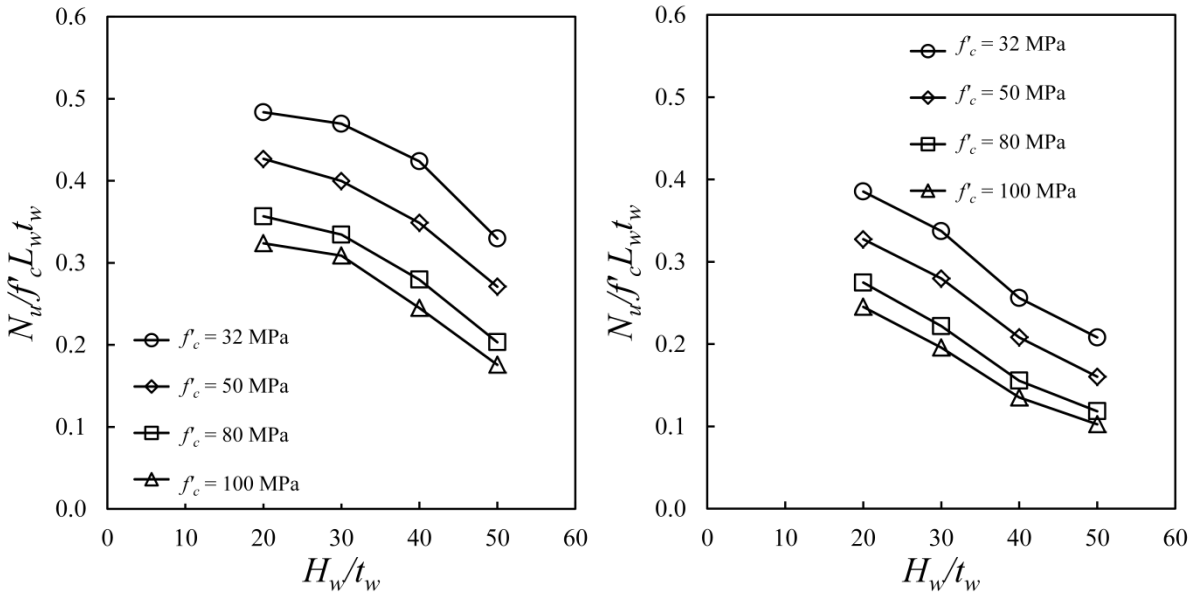

(a) $e = t_w/20$ (b) $e = t_w/6$

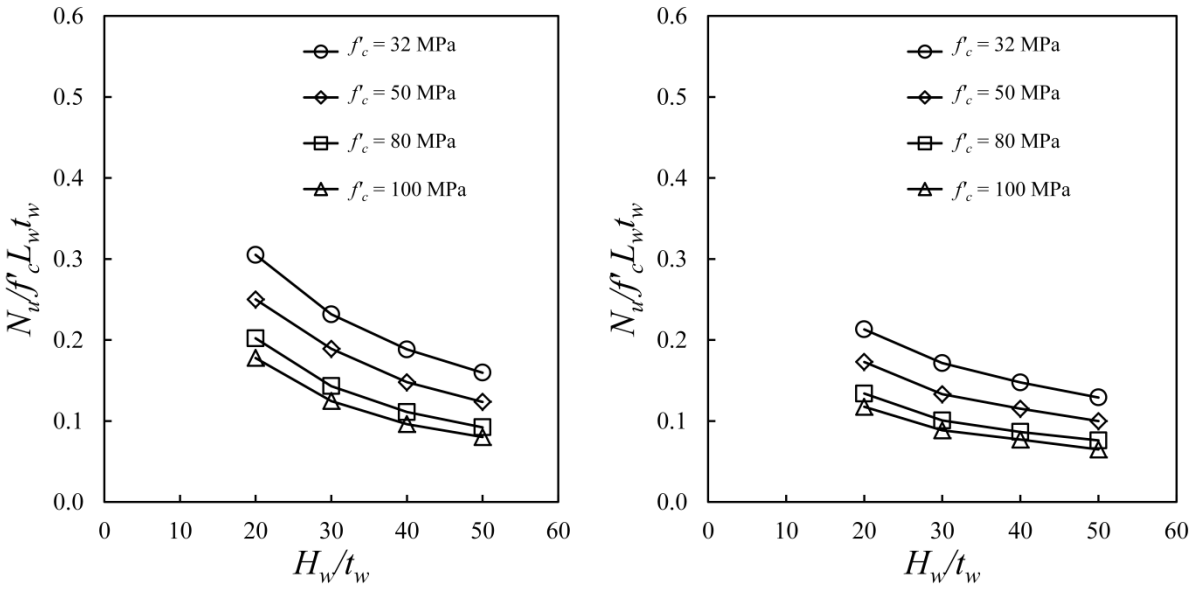

(c) $e = t_w/4$ (d) $e = t_w/3$

1 **FIGURE 12** Axial strength ratio versus slenderness ratio (H_w/L_w = 1.0, ρ = 0.31%)

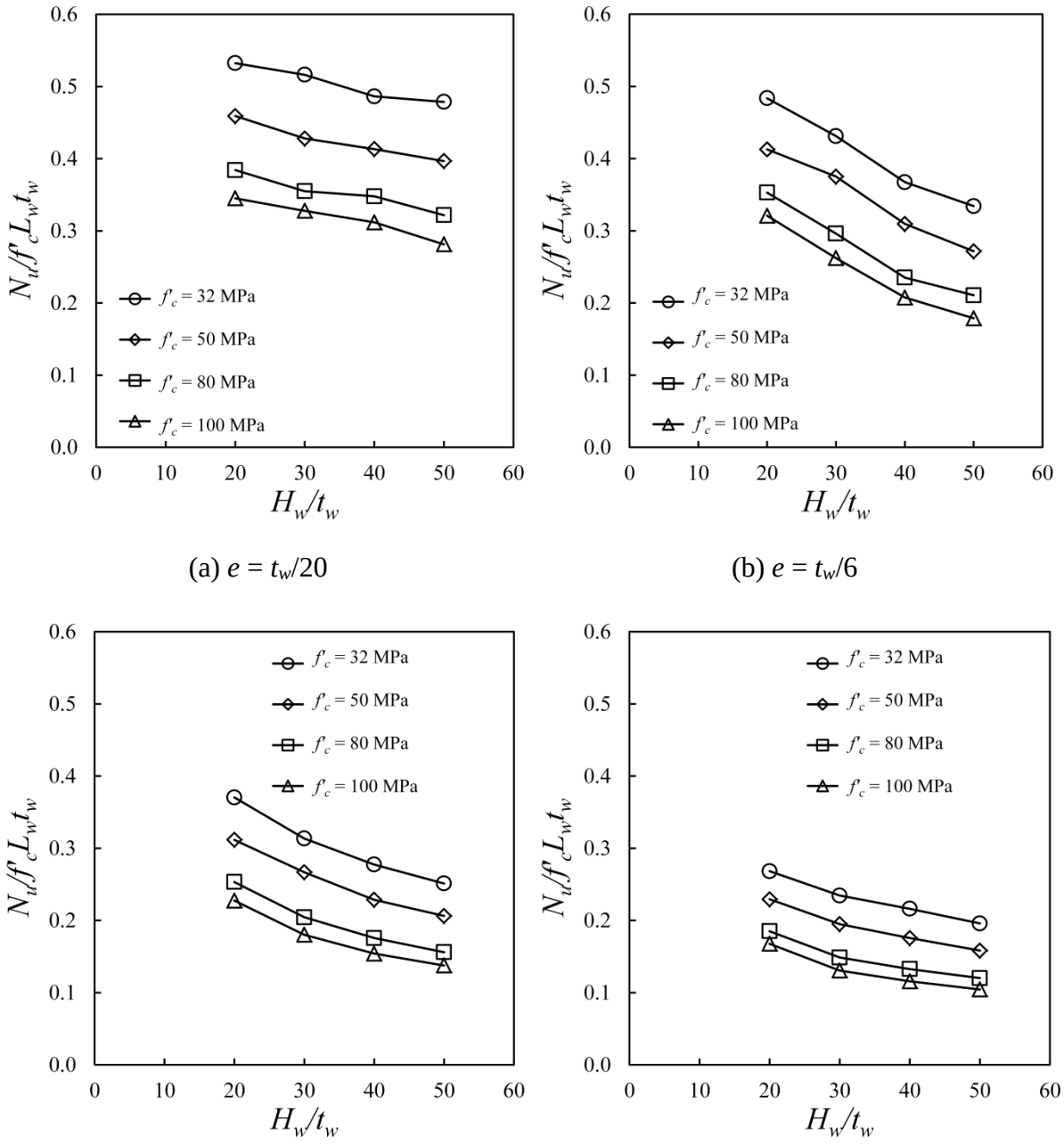

(a) $e = t_w/20$ (b) $e = t_w/6$

(c) $e = t_w/4$ (d) $e = t_w/3$

FIGURE 13 Axial strength ratio versus slenderness ratio (H_w/L_w = 2.0, ρ = 0.31%)

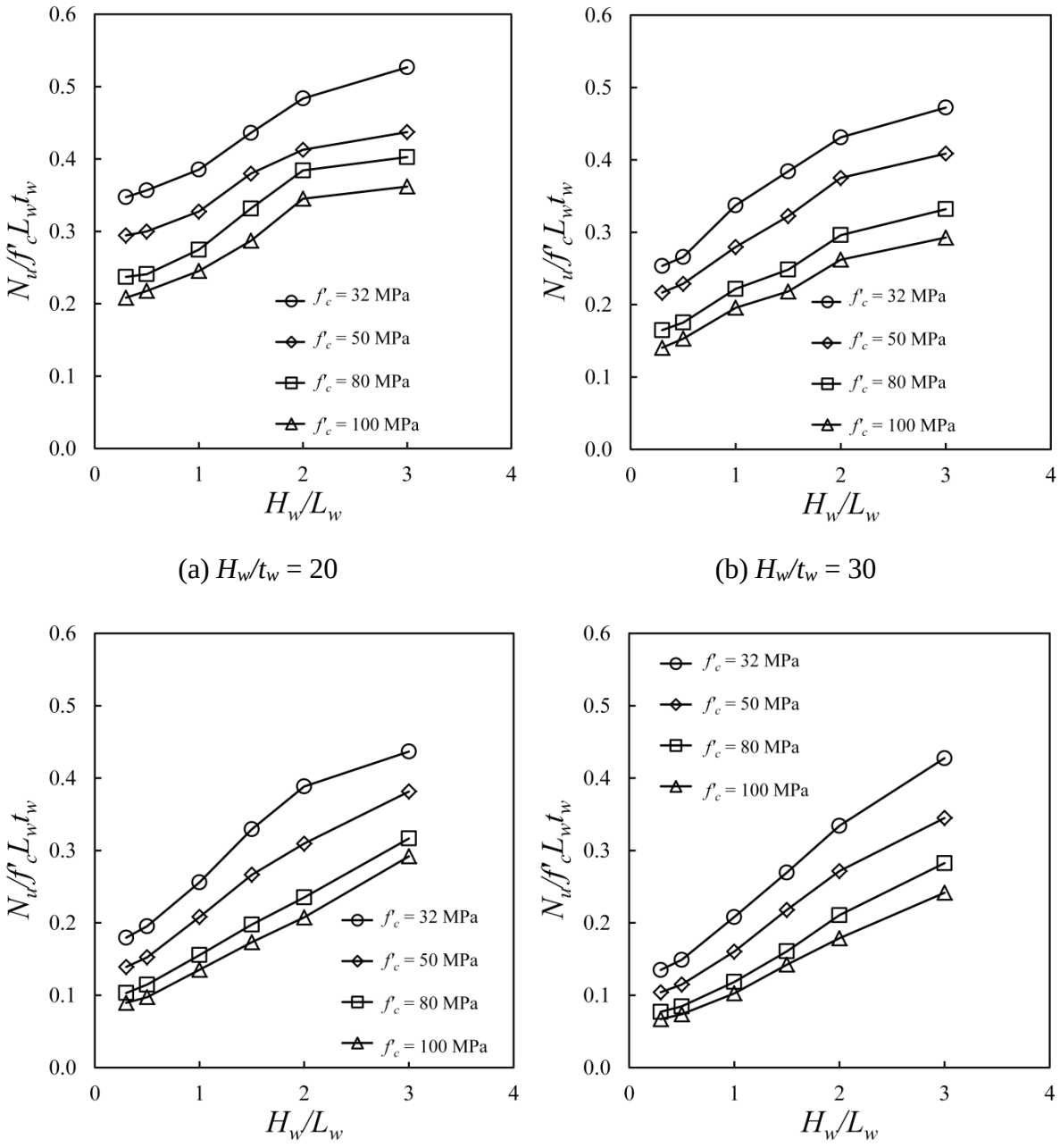

(a) H_w/t_w = 20 (b) H_w/t_w = 30

(c) H_w/t_w = 40 (d) H_w/t_w = 50

FIGURE 14 Axial strength ratio versus aspect ratio ($e = t_w/6$, $\rho = 0.31\%$)

TABLE 1 Design equations specified in standards

Code	Expression
EC2-04[2]	$N_d = \Phi \frac{f_c^{'}}{\gamma_c} L_w t_w$ (1) where ϕ (an equivalent value) = $1/\gamma_c$ = 0.67 (γ_c is equal to 1.5 for the ultimate limit state in the case of concrete under axial load); $\Phi = 1.14 \times \left(1 - 2\frac{e + e_a}{t_w}\right) - 0.02 \times \frac{H_{we}}{t_w} \le \left(1 - 2\frac{e + e_a}{t_w}\right)$; and $e_a = H_{we}/400$.
AS3600-09[3]	$N_d = \phi N_u = \phi 0.6 f_c^{'} L_w (t_w - 1.2e - 2e_a)$ (2) where ϕ = 0.6; and $e_a = H_{we}^2/(2500t_w)$.
ACI318-14[4]	$N_d = \phi N_u = \phi 0.55 f_c^{'} L_w t_w \left[1 - \left(H_{we}/32t_w\right)^2\right]$ (3) where ϕ = 0.65.

TABLE 2 Wall dimensions and concrete strengths

	Panel designation	Size of panel $H_w \times L_w \times t_w$ (mm)	f'_c (MPa)	H_w/t_w	H_w/L_w
Current	WS1a	1000 × 1000 × 40	47.6	25	1.0
	WS1b	1000 × 833.3 × 40	47.6	25	1.2
	WS1c	1000 × 625 × 40	47.6	25	1.6
	WS2a	1200 × 750 × 40	47.6	30	1.6
	WS2b	1200 × 600 × 40	47.6	30	2.0
	WS3a	1400 × 875 × 40	47.6	35	1.6
Doh et al[6]	TSNO	1200 × 1200 × 40	50.1	30	1.0
	TSHO	1200 × 1200 × 40	80.4	30	1.0
Ho and Doh[7]	WS1	1000 × 1200 × 40	58.8	25	0.83
	WS2	1200 × 1000 × 40	58.8	30	1.2
	WS3	1400 × 1000 × 40	58.8	35	1.4
	WS4	1600 × 1000 × 40	58.8	40	1.6

TABLE 3 Failure loads ($N_{uw,Test}$) and predicted loads of test panels by code equations, proposed equations and FE-Model

	Panel designation	$N_{uw,Test}$ (kN)	Eq. (1) (kN)	Eq. (2) (kN)	Eq. (4) (kN)	$N_{uw,FE\text{-}Model}$ (kN)	$\frac{\text{Eq. (1)}}{N_{uw,Test}}$	$\frac{\text{Eq. (2)}}{N_{uw,Test}}$	$\frac{\text{Eq. (4)}}{N_{uw,Test}}$	$\frac{N_{uw,FE\text{-}Model}}{N_{uw,Test}}$
Current	WS1a	499.1	346.1	451.2	459.9	588.5	0.69	0.90	0.92	1.18
	WS1b	450.6	327.0	407.8	407.9	502.5	0.73	0.91	0.91	1.12
	WS1c	398.4	309.1	354.8	343.9	393.7	0.78	0.89	0.86	0.99
	WS2a	410.3	228.1	311.5	383.6	423.2	0.56	0.76	0.93	1.03
	WS2b	355.9	258.4	311.8	345.5	353.5	0.73	0.88	0.97	0.99
	WS3a	471.7	99.5	205.9	415.0	472.7	0.21	0.44	0.88	1.00
Doh et al[6]	TSNO	502.2	159.0	312.8	501.0	624.5	0.32	0.62	1.00	1.24
	TSHO	809.3	255.1	502.0	619.9	767.0	0.32	0.62	0.77	0.95
Ho and Doh[7]	WS1	620.0	461.5	625.0	576.6	762.1	0.74	1.01	0.93	1.23
	WS2	500.1	224.3	373.9	486.0	589.0	0.45	0.75	0.97	1.18
	WS3	392.7*	50.2	196.4	479.0	555.9	0.13	0.50	1.22	1.42
	WS4	475.7	N/A#	34.1	482.3	528.3	N/A#	0.07	1.01	1.11
Mean**							0.55	0.71	0.92	1.09
Standard deviation**							0.21	0.27	0.07	0.11

*The specimen was damaged before testing (premature cracking due to handling)

Not applicable due to either the formulae giving negative results which implies zero axial strength or there being no guidelines in standards.

** The WS3 wall was excluded.

TABLE 4 Strength increase observation due to concrete strength (H_w/L_w = 1.0, ρ = 0.31%)

f'_c (MPa)	H_w/t_w	Failure load (kN)				Load ratio			
		$t_w/20$	$t_w/6$	$t_w/4$	$t_w/3$	$t_w/20$	$t_w/6$	$t_w/4$	$t_w/3$
32	20	6963.9	5549.8	4392.9	3068.7				
	30	4507.4	3238.0	2223.6	1646.3				
	40	3051.5	1844.0	1356.0	1062.6				
	50	1898.4	1198.2	920.0	743.1				
						N_u(50 MPa)/N_u(32 MPa)			
50	20	9601.9	7367.4	5627.9	3890.5	1.38	1.33	1.28	1.27
	30	5996.5	4195.3	2837.8	1996.7	1.33	1.30	1.28	1.21
	40	3923.3	2341.7	1663.2	1296.6	1.29	1.27	1.23	1.22
	50	2439.1	1442.9	1112.8	898.6	1.28	1.20	1.21	1.21
						N_u(80 MPa)/N_u(50 MPa)			
80	20	12842.1	9889.8	7274.3	4819.0	1.34	1.34	1.29	1.24
	30	8025.8	5323.2	3433.6	2416.7	1.34	1.27	1.21	1.21
	40	5031.6	2800.6	1998.5	1557.5	1.28	1.20	1.20	1.20
	50	2927.0	1705.9	1327.3	1094.6	1.20	1.18	1.19	1.22
						N_u(100 MPa)/N_u(80 MPa)			
100	20	14572.7	11039.6	8002.3	5286.4	1.13	1.12	1.10	1.10
	30	9266.8	5873.0	3739.5	2653.7	1.15	1.10	1.09	1.10
	40	5514.2	3040.9	2161.5	1733.0	1.10	1.09	1.08	1.11
	50	3163.2	1847.8	1443.8	1168.2	1.08	1.08	1.09	1.07

TABLE 5 Relationship of the axial strength ratio and the eccentricity for walls when the slenderness ratio approaches zero

	$e = t_w/20$	$e = t_w/6$	$e = t_w/4$	$e = t_w/3$
$N_u/f'_cL_wt_w$	0.765	0.567	0.425	0.283